Materials Transactions, Vol. 65, No. 7 (2024) pp. 736 to 743

他誌発表論文 再録
一般財団法人 軽金属学会
Materials Transactions, Vol.65, No.7(2024), pp. 736-743

Synthesis of TiC–Ti Composites via Mechanical Alloying/Spark Plasma Sintering Using Ti and C Powders

Ryo Tsukane[1], Kazuhiro Matsugi[2], Yong-Bum Choi[2] and Hiroyasu Tamai[1]

[1]*Tottori Institute of Industrial Technology, Tottori 689-3522, Japan*
[2]*Graduate School of Advanced Science and Engineering, Hiroshima University, Hiroshima 739-8527, Japan*

In this study, a TiC–Ti composite has been synthesized as a novel cermet without using rare elements like W, Co, and Ni. The mechanical properties of the prepared TiC–Ti composite are improved by utilizing Ti and C powders as raw materials in the mechanical alloying process. The effects of the non-equilibrium state during mechanical alloying on the characteristics of the composite have been analyzed. The results indicate that for short milling times, the addition of 25 mol% of C results in the Ti phase size in the sintered compact typically being on the order of several tens of micrometers, and unreacted C remains in the sample. A milling time of ≥21.6 ks affords a TiC–Ti composite containing approximately 80% fine TiC phase with an average size of 1–2 µm. As the milling progresses, the crystalline size of the Ti phase decreases, while the lattice strain increases. Prolonged milling improves the diffusion of C into Ti; a milling time of 36 ks at a low temperature of ∼700 K results in the formation of TiC as well as uniform diffusion of C throughout the Ti phase. Sintering the composite powder milled for 36 ks affords a Vickers hardness of approximately 700 Hv, which is similar to that of a TiC-35% Ni cermet.
[doi:10.2320/matertrans.MT-L2024002]

(Received January 24, 2024; Accepted April 17, 2024; Published June 25, 2024)

Keywords: *mechanical alloying, spark plasma sintering, cermet, composite, titanium carbide, titanium*

1. Introduction

Cermets and cemented carbides are extensively used in cutting tools and wear-resistant materials and predominantly rely on rare elements like W, Co, and Ni. These elements have limited reserves [1], and thus, development of alternative materials is necessary to minimize reliance on these elements. Ti is considered a promising alternative Ni owing to its abundance, which surpasses that of Ni, in the Earth's crust [2]. Therefore, numerous Ti matrix composites have been developed in recent years [3–5]. Additionally, the coefficient of thermal expansion of Ti closely aligns with that of TiC, and thus, a combination of these two materials is less prone to cracking during thermal contraction.

In traditional cermet fabrication, metal and ceramic powders are mixed and then sintered, often resulting in uneven metal phase distributions and a microstructure wherein hard particles are directly in contact with each other. Consequently, weak adhesion is observed at the metal/ceramic interface, and the mechanical properties of the material deteriorate. Mechanical alloying overcomes these limitations by ensuring uniform mixing of materials at the nanoscale and by activating chemical reactions via large strain application and surface area expansion [6, 7]. This method enables *in situ* synthesis of metal carbides and borides from metal and carbon (or boron) powders [8, 9]. Therefore, TiC–Ti composites with finely dispersed hard particles and strong metal/ceramic interfaces can be effectively prepared by a) mechanically alloying Ti and C powders in a controlled ratio and by b) solidifying the mixture using spark plasma sintering [10], which facilitates rapid sintering. In our previous study, we investigated the applicability of TiC–Ti composite prepared using this method to wear-resistant materials [11]. To control the properties of the composites, investigating the effects of different raw powder compositions and milling conditions is necessary.

In this study, a novel cermet, the TiC–Ti composite, which does not contain rare elements such as W, Co, and Ni, was synthesized. The study further explores the impact of non-equilibrium conditions during the mechanical alloying process on the properties of the composite, synthesized through a combination of mechanical alloying and spark plasma sintering of Ti and C powders.

2. Experimental Section

2.1 Mechanical alloying

A commercial Ti powder (<45 µm, oxygen concentration = 0.299 mass%, FUJIFILM Wako Pure Chemical Corp.) and C powder (mean particle size = 5 µm, Kojundo Chemical Laboratory Co., Ltd.) (Fig. 1) were mixed, and subsequently, 25 mol% of C was added to this mixed powder, which was then mechanically alloyed using a planetary ball mill (Fritsch P-6). Previous studies have suggested that TiC cermets can be fabricated by adding Ti as a binder at this C addition ratio [12]. According to the phase diagram, this rate of C addition is expected to yield a TiC:Ti ratio of approximately 8:2 in equilibrium [13]. The powders and tungsten carbide balls (25 balls, φ10 mm) were placed in an 80-mL tungsten carbide bowl inside a glove-box filled with Ar gas. The ball-to-powder mass ratio and milling speed were set at 5.8:1 and 500 rpm, respectively, and the mixture was milled up to 36 ks.

2.2 Spark plasma sintering process

The milled powder was then loaded into a cylindrical graphite die (φ20 mm), which was lined with a boron-nitride-coated interfacial graphite sheet to prevent any reaction with the die. The powder was subjected to spark plasma sintering (DR. SINTER SPS-3.20MK-4, Sumitomo Coal Mining Co.) under vacuum at 1273 K with a heating rate and dwell time of 1.68 K/s and 300 s, respectively. A uniaxial pressure of 35 MPa was applied to the powder during the sintering process.

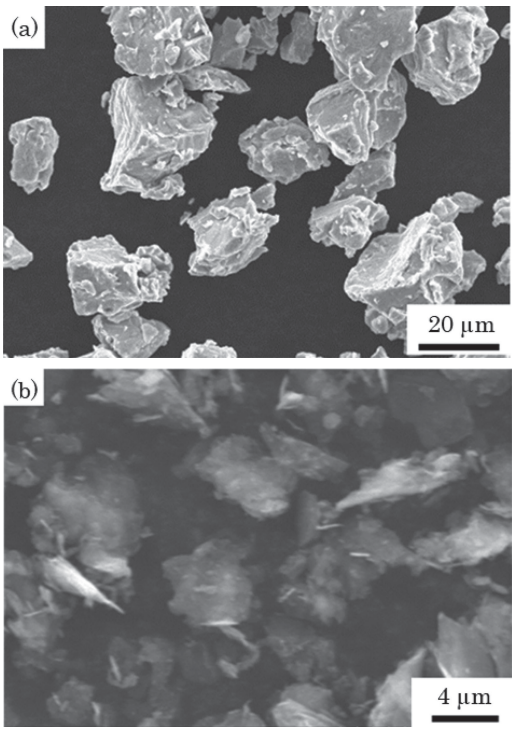

Fig. 1 SEM images of the (a) Ti powder and (b) C powder.

2.3 Material characterization

The morphologies and microstructures of the powders were analyzed by field-emission scanning electron microscopy (SEM; SU5000, Hitachi High-Tech). The phase composition was determined by X-ray diffraction (XRD) analysis (Ultima IV, Rigaku) using Cu–Kα radiation at 40 kV and 40 mA. The internal lattice strain and crystalline size were estimated from the broadened XRD peaks using the Williamson–Hall method as follows [14]:

$$\beta \cos\theta = 0.9\lambda/D + \varepsilon \sin\theta \quad (1)$$

where β represents the full width at half maximum of the XRD peaks, θ denotes the diffraction angles, λ is the wavelength of X-rays (m), D indicates the crystalline size (m), and ε is the internal lattice strain. The XRD analysis data were used to estimate the lattice parameters for different (hkl) reflections of the face-centered cubic TiC phase formed during the milling. These XRD data were fitted using Nelson–Riley extrapolation function, and more accurate lattice parameters were calculated by extrapolating these results to $\theta = \pi/2$ [15]. The milled powders were characterized using differential scanning calorimetry (DSC; DSC6300, Hitachi High-Tech Science Co.) under a constant Ar flow of 200 mL/min at a heating rate of 20 K/min. The hardness of the samples was measured using a micro-Vickers hardness testing machine (HM-220D, Mitsutoyo) with a load of 4.9 N for a constant contact time of 10 s.

3. Results and Discussion

3.1 Mechanical alloying of the Ti–C mixed powders

Figure 2 illustrates the XRD patterns of the powders milled for different durations. The XRD pattern of the unmilled powder shows distinct diffraction peaks of the Ti and C phases. After 3.6 ks of milling, the diffraction peak of C disappears, while those of Ti broaden, and their intensity decreases as the milling progresses. The powder milled for 21.6 ks displays broad and weak TiC diffraction peaks, whose intensity increases. During the mechanical alloying of a Ti–C system, TiC rapidly forms via a mechanically induced self-propagating reaction (MSR) depending on the milling conditions. MSR typically occurs when the C content is approximately 50 mol% [16]. In our study, because of the addition of 25 mol% of C, MSR does not occur, and TiC is gradually synthesized via atomic diffusion.

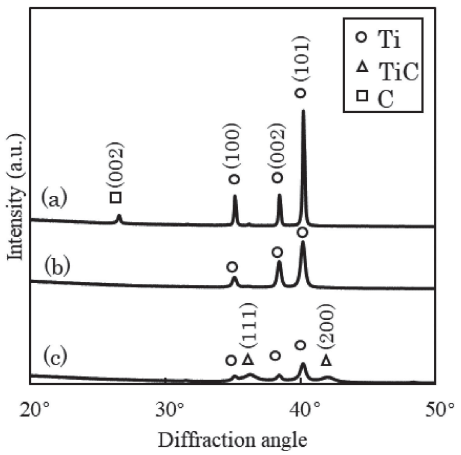

Fig. 2 XRD patterns of the powders milled for (a) 0 ks, (b) 3.6 ks, and (c) 36 ks.

Figure 3 presents the backscattered electron images of the milled powders, revealing the morphological changes at various milling stages. In Fig. 3(a), the SEM images of the powders milled for 3.6 ks show distinct Ti and C particles. The Ti powder appears slightly flattened and aggregated with the C powder. No C peak is observed in the XRD pattern owing to the fine grinding of C and its entrapment between the Ti particles. However, the difference between the particles is evident in the SEM images. The powder milled for 10.8 ks shows repeated fracturing, and cold welding results in the formation of a lamellar structure as depicted in Fig. 3(b). After milling for 36 ks, the Ti phase becomes thin with a narrow interlayer spacing as shown in Fig. 3(c).

Figure 4 shows the internal strains and crystalline sizes of the Ti phase in the milled powders. The internal lattice strain rapidly increases from 0.027% to 0.28% after 3.6 ks of milling, and then gradually increases with increasing milling time, reaching 0.4% at 36 ks. The crystalline size of the Ti phase sharply decreases from 57 to 40 nm after the initial 3.6 ks of milling and then gradually decreases as the milling time increases.

The DSC curves of the milled powders are illustrated in Fig. 5. The curve for the unmilled powder does not any peak, whereas those of the powders milled for 3.6 and 36 ks exhibit distinct peaks. The powder milled for 3.6 ks exhibits an exothermic peak at approximately 1100 K; in contrast, the powder milled for 36 ks shows a peak at approximately 700 K. This result is attributed to the heat of formation of TiC and aligns with the XRD results of the powder subjected to

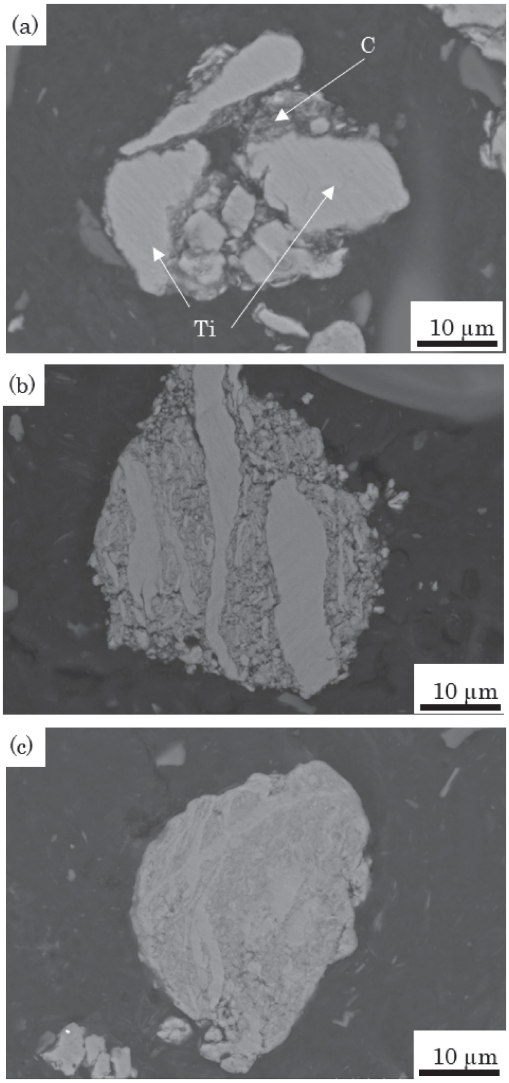

Fig. 3 Cross-sectional backscattered electron micrographs of the powders milled for (a) 3.6 ks, (b) 10.8 ks, and (c) 36 ks.

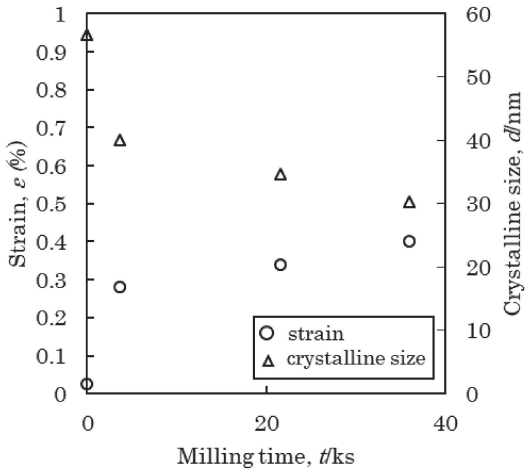

Fig. 4 Analyzed lattice strain and crystallite sizes of the powders milled for different times.

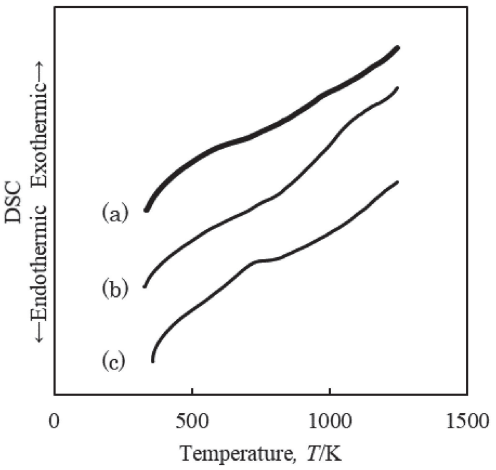

Fig. 5 DSC curves of the powders milled for (a) 0 ks, (b) 3.6 ks, and (c) 36 ks.

DSC. These findings indicate that prolonged milling reduces the temperature required for TiC synthesis. Bhattacharya and Arzt computed diffusivity by considering dislocation accumulation [17] using:

$$D = D_l \exp(-Q_l/RT) + \beta b^2 \rho D_c \exp(-Q_c/RT) \quad (2)$$

where D_l and D_c represent the lattice and core diffusion constants (m^2/s) of the material, respectively; Q_l and Q_c denote the activation energies for lattice and core diffusion (J/mol), respectively; b is the Burgers vector; ρ represents the dislocation density; and β is the core diffusivity factor. Equation (2) illustrates that diffusivity increases with increasing dislocation density. The influence of crystalline size on diffusivity is expressed by the following equation [18]:

$$D_{eff} = (1 - F)D_l + FD_b \quad (3)$$

where D_{eff} is the effective diffusivity (m^2/s), F is the area fraction of short-circuit paths (such as grain boundaries) in a plane perpendicular to the diffusion direction, and D_b is the grain boundary diffusivity (m^2/s). Because D_b is typically larger than D_l, D_{eff} increases with decreasing crystalline size.

Figure 4 shows that as milling time increases, the strain within the material increases, while the crystalline size decreases. Consequently, the milled powder exhibits a large diffusivity and chemical reactivity. Therefore, prolonged milling reduces the temperature required for synthesizing TiC; this result is evident from the decrease in the TiC formation temperature as is shown in the DSC curves (Fig. 5). This relationship highlights the importance of mechanical milling for optimizing the TiC synthesis conditions.

3.2 Characteristics of the sintered compacts

Figure 6 shows the XRD patterns of the milled powders subjected to spark plasma sintering. The profile of the unmilled mixed sample subjected to sintering shows peaks corresponding to Ti, TiC, and C, revealing the presence of unreacted C. In contrast, only Ti and TiC peaks appear in the XRD patterns of the milled samples subjected to sintering. Figure 7 shows the relationship between milling time and the

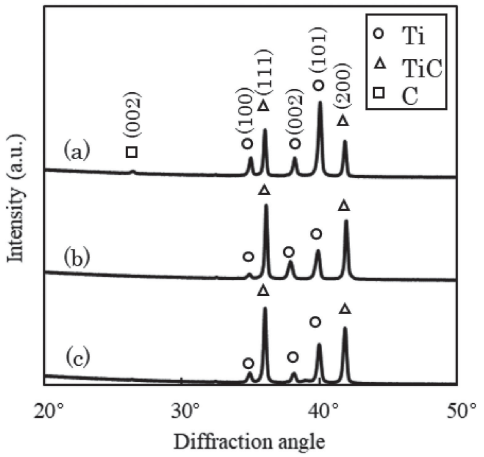

Fig. 6 XRD patterns of the sintered compacts derived from the powders milled for (a) 0 ks, (b) 3.6 ks, and (c) 36 ks.

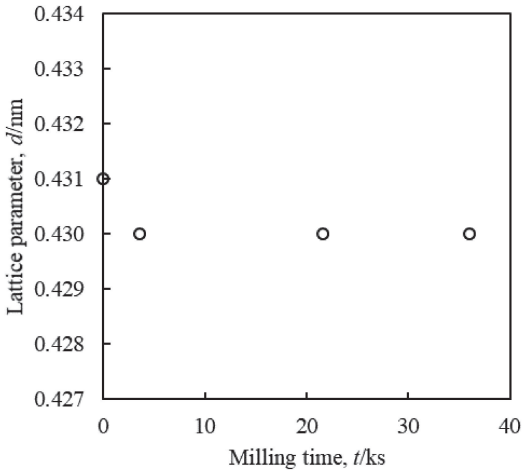

Fig. 7 Graph depicting the relationship between milling time and the lattice parameter of the sintered compacts.

lattice parameter of sintered TiC. Evidently, the lattice parameter is 0.430 nm irrespective of the milling time. Further, the stoichiometric ratio x of TiC_x is correlated to the lattice parameter, and for a lattice parameter of 0.430 nm, the estimated x of the synthesized TiC is 0.5.

The backscattered electron images of the microstructures of the sintered compacts, shown in Fig. 8, indicate the presence of three distinct phases. Based on energy-dispersive X-ray spectroscopy and XRD analysis results, we identify these phases as: (1) pores or carbon (black component), (2) Ti phase (brighter contrast), and (3) TiC phase (darker contrast). The volume ratios of the TiC phases, determined through image analysis and shown in Fig. 9, indicate that the unmilled sample contains ~50% of TiC by volume. In the samples milled for 3.6 and >21.6 ks, the TiC volume ratios increase to 67% and ~80%, respectively. In the unmilled samples (Fig. 8(a)), the TiC phase is distributed over a region of several tens of micrometers, with unreacted C interspersed within the TiC phase. After milling for 3.6 ks, although the size of the Ti phase remains unchanged, and the phase appears flattened (Fig. 8(b)), a small amount of unreacted C is still detected in the TiC phase. This unreacted C is finely distributed and thus cannot be detected in the XRD patterns (Fig. 6).

The samples milled for 21.6 (Fig. 8(c)) and 36 ks (Fig. 8(d)) show more refined structures, with TiC phase sizes of ~2 (Fig. 8(e)) and 1 μm (Fig. 8(f)), respectively. This result indicates that prolonged milling produces fine microstructures such that the phase size decreases with increasing milling time. In addition, unreacted C is still detected in the sample milled for 21.6 ks (Fig. 8(e)). This observation confirms that extended milling facilitates the reaction between Ti and C as well as refines the microstructure, thus enhancing the overall properties of the material.

The process of microstructure formation during the sintering of unmilled or short-duration-milled powder (3.6 ks) involves several key stages. The microstructure evolution during sintering is schematically shown in Fig. 10(a). Initially, C present around the Ti phase diffuses into Ti with increasing temperatures. However, the diffusion coefficient of C in α-Ti is low (approximately 10^{-16} cm^2/s at 600 K) [19], and because of this low diffusion rate, minimal diffusion occurs at low temperatures. When Ti undergoes phase transformation to β-Ti, the diffusion coefficient of C in Ti significantly increases to approximately 10^{-10} cm^2/s [20]. Consequently, the diffusion of C into Ti and formation of TiC predominantly occur after this β-transformation.

The absence of exothermic peak in the DSC curves (Fig. 5) indicate that only a limited amount of TiC is formed during the sintering of the unmilled powder. In contrast, the DSC curve of the powder milled for 3.6 ks exhibits an exothermic peak around the β-transformation temperature, which is approximately 1100 K. In regions outside the Ti phase, where the C concentration is high, C reacts with Ti to form TiC around the Ti phase. Subsequently, C diffuses through the newly formed TiC layer and reacts with Ti at the Ti/TiC interface, thereby increasing the amount of TiC formed. The large size of the Ti particles prior to sintering impedes the diffusion of C to the center of these particles. Additionally, after sintering, Ti is unevenly distributed, forming large lumps.

The amount of TiC formed in the sample milled for 3.6 ks is higher than that formed in the unmilled sample. This increase in the TiC amount can be attributed to the enhanced reactivity of the powder due to the accumulated lattice strain and reduced crystalline size. Therefore, the milling process plays a crucial role in modifying the microstructural properties of the powder, and these modified microstructure in turn affects the diffusion dynamics and efficiency of TiC formation during sintering.

For the powders subjected to prolonged milling (milling times: 21.6 and 36 ks), the microstructure formation during sintering follows a distinct process. A schematic of the microstructure evolution during sintering is shown in Fig. 10(b). The milled powder develops a lamellar structure with a notably small interlayer spacing as shown in Fig. 3(c). C, which is initially present in the surrounding of the thin Ti layers, diffuses into Ti as the temperatures increases during the sintering. As the milling time is increased, the crystalline size decreases, the amount of accumulated lattice strain increases, and the thickness of the Ti layer decreases.

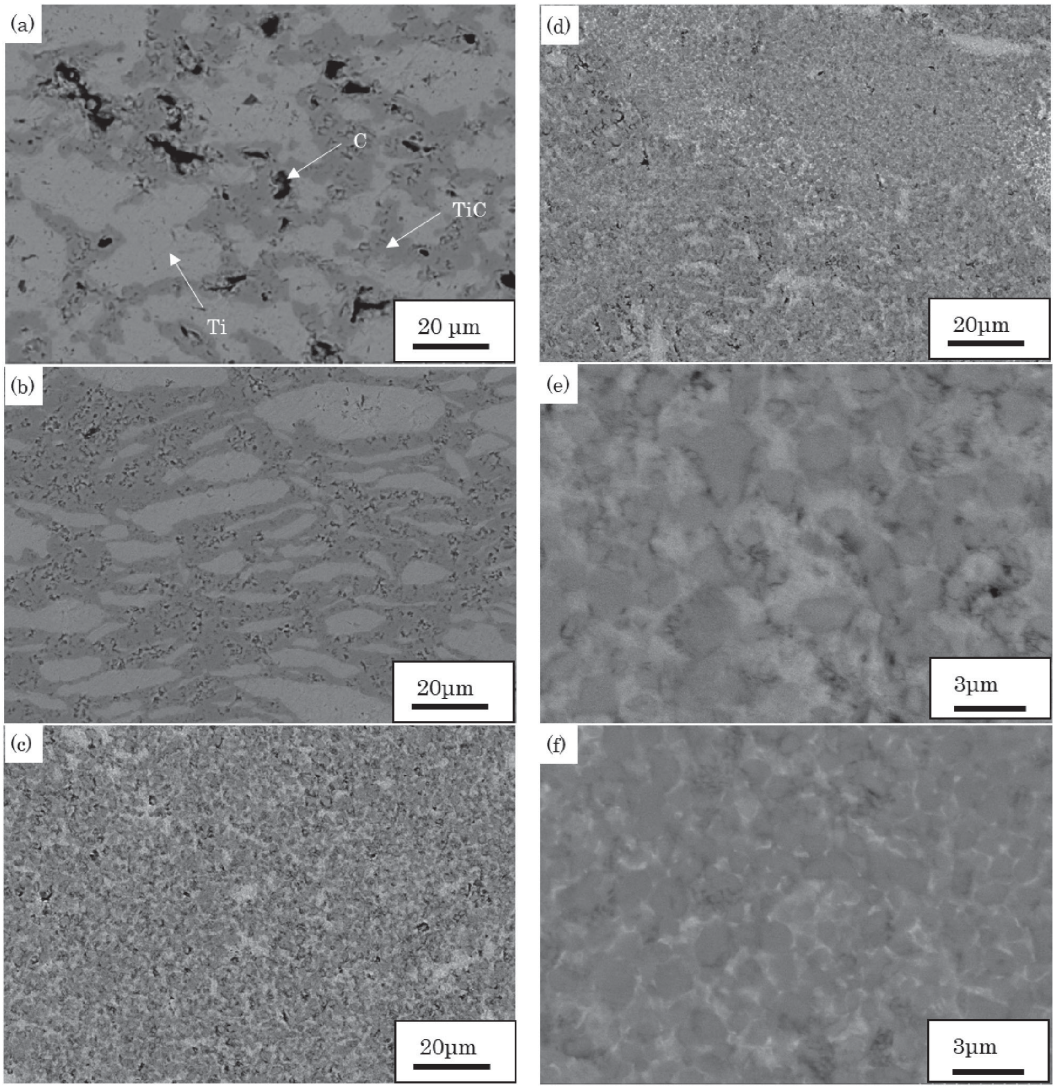

Fig. 8 Cross-sectional backscattered electron micrographs of the sintered compacts derived from the powders milled for (a) 0 ks, (b) 3.6 ks, (c) 21.6 ks, (d) 36 ks. High-magnification views of the samples milled for (e) 21.6 ks and (f) 36 ks.

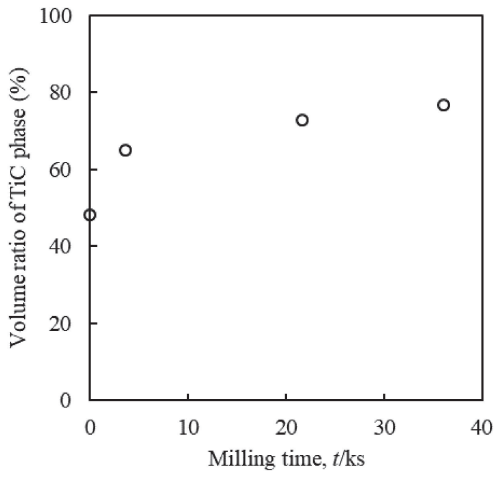

Fig. 9 Graph depicting the relationship between milling time and the volume ratio of the TiC phase in the sintered compacts.

Therefore, as the milling time increases, the number of grain boundaries and lattice defects, which serve as diffusion paths for C, increases [21]. Further, as the temperature increases, C disperses uniformly throughout the Ti. With a further increase in temperature, fine TiC is formed. The DSC results (Fig. 5) indicate that TiC forms occurs at approximately 700 K in the sample milled for 36 ks.

Figure 11 displays the Vickers hardness values of the sintered compacts. The Vickers hardness value of the TiC–Ti composite prepared by sintering the unmilled powder is approximately 400 Hv. The composite obtained from the powder milled for 3.6 ks shows the highest Vickers hardness value of 930 Hv. After milling for 21.6 ks, the Vickers hardness value of the sample remains almost constant at 690 Hv, which is lower than those of WC–Co and WC–Ni alloys, but comparable with that of a TiC-35% Ni cermet [22, 23]. SEM images of the indentations on the sintered compacts prepared from powders milled for 3.6 and 36 ks are displayed in Fig. 12. Although the composite obtained from

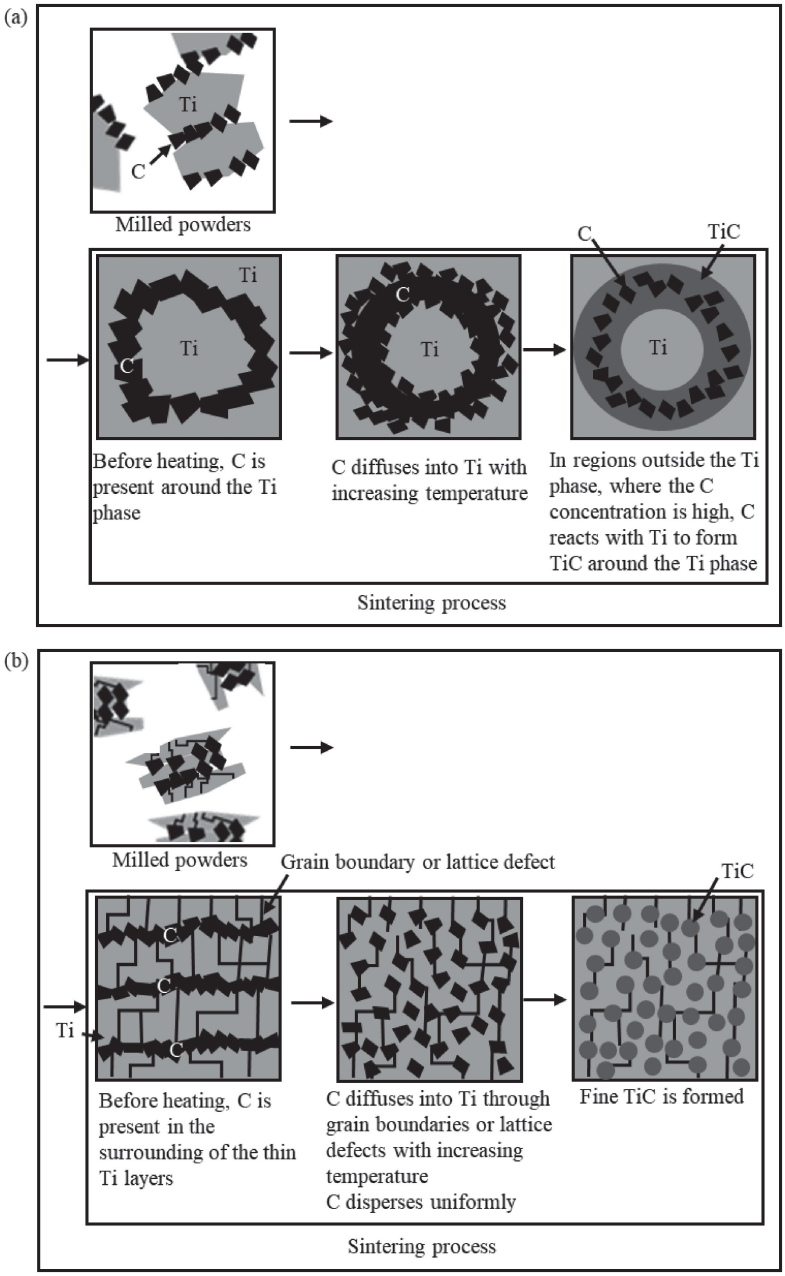

Fig. 10 Schematic of the microstructure evolution during the sintering of the powders milled for (a) short time (3.6 ks) and (b) long times (21.6 and 36 ks).

the powder milled for 3.6 ks shows the highest hardness value, cracks appear in the indentations of this composite (Fig. 12(a)). In this sample, TiC is not finely dispersed; instead, it shows a continuous dispersion profile. Because of this continuous TiC, the depth penetrated by the indenter is small. Thus, despite its high hardness value, the sample lacks toughness. Conversely, cracks are not visible in the indentations of the composite obtained from the powder milled for 36 ks (Fig. 12(b)). This result indicates that the microstructure of this composite possesses excellent fracture toughness.

This difference in the microstructural characteristics and mechanical properties of the composites derived from the unmilled and long-term-milled powders underscores the significant impact of the milling process. Overall, longer milling times promote efficient synthesis of TiC at low temperatures as well as contribute to the development of composites with finer microstructures and enhanced mechanical properties, such as increased hardness and improved fracture toughness.

4. Conclusion

A TiC–Ti composite was successfully synthesized by a combination of mechanical alloying and spark plasma sintering using Ti and C powders as raw materials. This novel cermet composition effectively circumvents the use of rare elements like W, Co, and Ni. The study was focused on

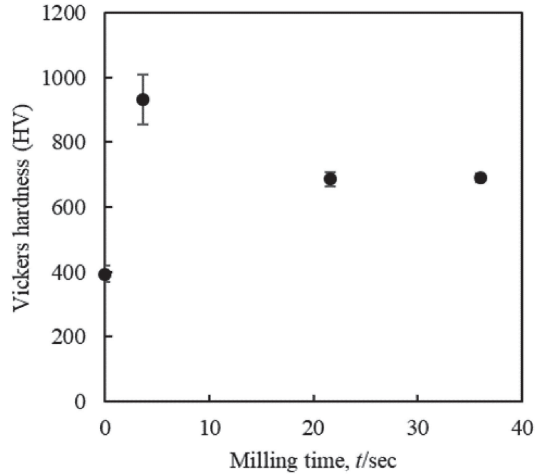

Fig. 11 Graph depicting the relationship between milling time and Vickers hardness.

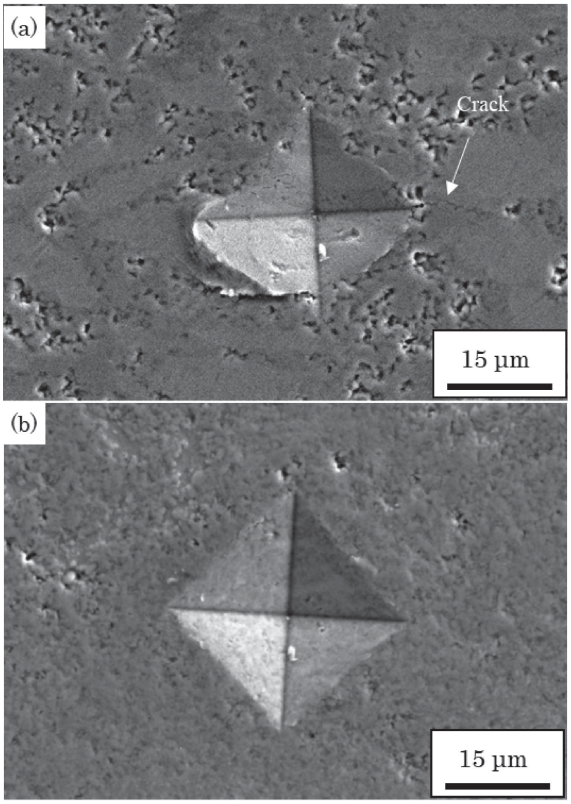

Fig. 12 SEM images of indentations on the TiC–Ti composites sintered from the powders milled for (a) 3.6 ks and (b) 36 ks.

assessing the impact of non-equilibrium conditions during the mechanical alloying stage on the properties of the resultant composites. The key conclusions drawn from the study findings are summarized below:

(1) As the milling time increased, the crystalline size of the Ti phase decreased, while the lattice strain increased, resulting in enhanced diffusion of C into Ti. Consequently, TiC was successfully synthesized at a low temperature; specifically, TiC formation was achieved at approximately 700 K in the powders milled for 36 ks.

(2) Short milling durations resulted in the formation of large Ti phase sizes of the order of several tens of micrometers, within the sintered compact, and unreacted C remained in the composite. However, milling for ≥21.6 ks led to the formation of a TiC–Ti composite containing ~80% of finely dispersed TiC phase, whose average particle size was in the range of 1–2 µm.

(3) The TiC–Ti composite, sintered from powder milled for 36 ks, exhibited a Vickers hardness value of approximately 700 Hv, which was comparable with that of a TiC-35% Ni cermet.

These findings underscore the effectiveness of extended milling in refining the microstructural features of the composite and thus enhance its mechanical properties. These results demonstrate that the composite prepared in this study is a viable alternative to rare-earth-containing cermets.

Acknowledgments

This study received support from the JKA Public-Interest-Incorporated Foundation. We are thankful for the subsidies obtained from bicycle and other machine industry promotion projects, which helped in procuring some of the equipment essential for this study. Additionally, the financial assistance provided by the Amada Foundation is greatly appreciated. The authors would also like to express their heartfelt thanks to Toshiyuki Ueno, Shimane Institute for Industrial Technology, for his invaluable assistance with the spark plasma sintering process.

REFERENCES

[1] Y. Hamada and N. Sato: Recycling of Rare Metals, Shigen-To-Sozai **107** (1991) 109–118.
[2] T. Okabe: Smelting, Refining, and Recycling of Titanium, Materia Japan **58** (2019) 176–180.
[3] T. Furuta, K. Shiina, Y. Ueda, S. Shimazaki and K. Nakamura: Effect of C and Al Elements on High Specific Resistance and High Rigidity of Ultra-High Strength $TiC_{(1-X)}$/Ti Metal Matrix Composites Fabricated by Blended Elemental Reactive Sintering, Mater. Trans. **60** (2019) 1864–1872.
[4] I. Shon, H. Kwon and H. Jo: Properties and Rapid Consolidation of Nanostructured TiC and TiC–TiAl Hard Materials by High-Frequency Induction Heating, Mater. Trans. **55** (2014) 1363–1366.
[5] T. Yamaguchi, H. Hagino, Y. Michiyama and A. Nakahira: Sliding Wear Properties of Ti/TiC Surface Composite Layer Formed by Laser Alloying, Mater. Trans. **56** (2015) 361–366.
[6] C. Suryanarayana: Mechanical alloying and milling, Prog. Mater. Sci. **46** (2001) 1–184.
[7] T. Ohno and M. Kubota: Fabrication of high strength pure titanium by mechanical milling and spark plasma sintering and its properties, J. JILM **59** (2009) 659–665.
[8] L. Takacs: Self-sustaining reactions induced by ball milling, Prog. Mater. Sci. **47** (2002) 355–414.
[9] G. Liu, J. Li and K. Chen: Combustion synthesis of refractory and hard materials: A review, Int. J. Refract. Hard Met. **39** (2013) 90–102.
[10] O. Yanagisawa, T. Hatayama and K. Matsugi: Recent Research on Spark Sintering Process, Materia Japan **33** (1994) 1489–1496.
[11] R. Tsukane, K. Matsugi, Y. Choi and H. Tamai: Oxidation/Carburization Behavior of TiC–Ti Composites and Improved Wear Resistance through Surface Modification, Mater. Trans. **65** (2024) 323–330.
[12] R. Tsukane, K. Matsugi, Y. Choi and H. Tamai: Book of abstracts of NERPS 2024 Conference in Hiroshima, Japan.
[13] P. Xiao and B. Derby: Wetting of titanium nitride and titanium carbide by liquid metals, Acta Mater. **44** (1996) 307–314.

[14] G.K. Williamson and W.H. Hall: X-ray line broadening from filed aluminium and wolfram, Acta Metall. **1** (1953) 22–31.
[15] J.B. Nelson and D.P. Riley: An experimental investigation of extrapolation methods in the derivation of accurate unit-cell dimensions of crystals, Proc. Phys. Soc. **57** (1945) 160–177.
[16] B.H. Lohse, A. Calka and D. Wexler: Effect of starting composition on the synthesis of nanocrystalline TiC during milling of titanium and carbon, J. Alloy. Compd. **394** (2005) 148–151.
[17] A.K. Bhattacharya and E. Arzt: Diffusive reaction during mechanical alloying of intermetallics, Scr. Metall. Mater. **27** (1992) 635–639.
[18] H.V. Atkinson and B.A. Rickinson: *The Adam Hilger Series on New Manufacturing Processes and Materials*, ed. by J. Wood, (Adam Hilger, Bristol, 1991) pp. 34–38.
[19] L. Scotti and A. Mottura: Interstitial diffusion of O, N, and C in α-Ti from first-principles: Analytical model and kinetic Monte Carlo simulations, J. Chem. Phys. **144** (2016) 084701.
[20] H. Nakajima and M. Koiwa: Diffusion in Titanium, ISIJ Int. **31** (1991) 757–766.
[21] H. Mehrer: *Diffusion in Solids*, Trans. S. Fujikawa, (Maruzen Publishing Co., Ltd., 2012) pp. 561–636.
[22] H. Suzuki and T. Yamamoto: Effects of Carbon Content on Some Properties of WC-10%(Co-Ni) Cemented Carbides, J. Jpn. Soc. Powder Powder Metallurgy **15** (1968) 68–71.
[23] M. Sugiyama and H. Suzuki: Studies on Vacuum-Sintering of TiC-Ni Cermets, J. Japan Inst. Metals **24** (1960) 689–692.